J|A|C|S
A R T I C L E S

Mechanistic Study on the Replacement Reaction between Silver Nanostructures and Chloroauric Acid in Aqueous Medium

Yugang Sun and Younan Xia*

Contribution from the Department of Chemistry, University of Washington, Seattle, Washington 98195-1700

Received November 27, 2003; E-mail: xia@chem.washington.edu

Abstract: The replacement reaction between silver nanostructures and an aqueous $HAuCl_4$ solution has recently been demonstrated as a versatile method for generating metal nanostructures with hollow interiors. Here we describe the results of a systematic study detailing the morphological, structural, compositional, and spectral changes involved in such a heterogeneous reaction on the nanoscale. Two distinctive steps have been resolved through a combination of microscopic and spectroscopic methods. In the first step, silver nanostructure (i.e., the template) is dissolved to generate gold atoms that are deposited epitaxially on the surface of each template. Silver atoms also diffuse into the gold shell (or sheath) to form a seamless, hollow nanostructure with its wall made of Au−Ag alloys. The second step involves dealloying, a process that selectively removes silver atoms from the alloyed wall, induces morphological reconstruction, and finally leads to the formation of pinholes in the walls. Reaction temperature was found to play an important role in the replacement reaction because the solubility constant of AgCl and the diffusion coefficients of Ag and Au atoms were both strongly dependent on this parameter. This work has enabled us to prepare metal nanostructures with controllable geometric shapes and structures, and thus optical properties (for example, the surface plasmon resonance peaks could be readily shifted from 500 to 1200 nm by controlling the ratio between Ag and $HAuCl_4$).

1. Introduction

Metal nanostructures have been extensively studied for many decades because of their use in applications such as catalysis, photography, optics, electronics, optoelectronics, information storage, biological and chemical sensing, and surface-enhanced Raman scattering (SERS).[1−5] In general, the intrinsic properties of a metal nanostructure can be tuned by controlling its shape as well as structure (hollow vs solid).[6] For example, the surface plasmon resonance (SPR) peak of gold or silver nanorods can shift from the visible to near-infrared (near-IR) region by increasing their aspect ratios.[7] It has also been demonstrated that gold nanoshells formed on the surface of silica spheres can be used to tune their SPR peaks from 600 to 1200 nm by varying the wall thickness and/or the core size.[8] By processing metal nanostructures into hollow ones, their performance could be further improved due to their relatively lower densities and higher surface areas than the solid counterparts. For example, nanoshells made of Pd have recently been demonstrated as an effective, recoverable catalyst for the Suzuki coupling reactions,[9] while solid Pd nanoparticles usually lose their catalytic activities after one cycle of operation.[10]

(1) Reviews: (a) Halperin, W. P. *Rev. Mod. Phys.* **1986**, *58*, 533. (b) Templeton, A. C.; Wuelfing, W. P.; Murray, R. W. *Acc. Chem. Res.* **2000**, *33*, 27. (c) Lam, D. M.-K.; Rossiter, B. W. *Sci. Am.* **1991**, *265* (5), 80. (d) Lewis, L. N. *Chem. Rev.* **1993**, *93*, 2693. (e) Murray, C. B.; Sun, S.; Doyle, H.; Betley, T. *Mater. Res. Soc. Bull.* **2001**, *26*, 985.

(2) Optics and catalysis: (a) Novak, J. P.; Brousseau, L. C., III; Vance, F. W.; Johnson, R. C.; Lemon, B. I.; Hupp, J. T.; Feldheim, D. L. *J. Am. Chem. Soc.* **2000**, *122*, 12029. (b) Murphy, C. J.; Jana, N. R. *Adv. Mater.* **2002**, *14*, 80. (c) Kim, F.; Song, J. H.; Yang, P. *J. Am. Chem. Soc.* **2002**, *124*, 14316. (d) Nicewarner-Peña, S. R.; Freeman, R. G.; Reiss, B. D.; He, L.; Peña, D. J.; Walton, I. D.; Cromer, R.; Keating, C. D.; Natan, M. J. *Science* **2001**, *294*, 137. (e) Ahmadi, T. S.; Wang, Z. L.; Green, T. C.; Henglein, A.; El-Sayed, M. A. *Science* **1996**, *272*, 1924. (f) Teng, X.; Black, D.; Watkins, N. J.; Gao, Y.; Yang, H. *Nano Lett.* **2003**, *3*, 261.

(3) Electronics and optoelectronics: (a) Chen, S.; Yang, Y. *J. Am. Chem. Soc.* **2002**, *124*, 5280. (b) El-Sayed, M. A. *Acc. Chem. Res.* **2001**, *34*, 257. (c) Maier, S. A.; Brongersma, M. L.; Kik, P. G.; Meltzer, S.; Requicha, A. A. G.; Atwater, H. A. *Adv. Mater.* **2001**, *13*, 1501. (d) Kamat, P. V. *J. Phys. Chem. B* **2002**, *106*, 7729.

(4) Sensing and clinical diagnostics: (a) Tkachenko, A. G.; Xie, H.; Coleman, D.; Glomm, W.; Ryan, J.; Anderson, M. F.; Franzen, S.; Feldheim, D. L. *J. Am. Chem. Soc.* **2003**, *125*, 4700. (b) Taton, T. A.; Mirkin, C. A.; Letsinger, R. L. *Science* **2000**, *289*, 1757. (c) Thanh, N. T. K.; Rosenzweig, Z. *Anal. Chem.* **2002**, *74*, 1624. (d) Kim, Y.; Johnson, R. C.; Hupp, J. T. *Nano Lett.* **2001**, *1*, 165. (e) Nath, N.; Chilkoti, A. *Anal. Chem.* **2002**, *74*, 504. (f) Roll, D.; Malicka, J.; Gryczynski, I.; Cryczynski, Z.; Lakowicz, J. R. *Anal. Chem.* **2003**, *75*, 3440.

(5) SERS: (a) Tessier, P. M.; Velev, O. D.; Kalambur, A. T.; Rabolt, J. F.; Lenhoff, A. M.; Kaler, E. W. *J. Am. Chem. Soc.* **2000**, *122*, 9554. (b) Nie, S.; Emory, S. R. *Science* **1997**, *275*, 1102. (c) Dick, L. A.; McFarland, A. D.; Haynes, C. L.; Van Duyne, R. P. *J. Phys. Chem. B* **2002**, *106*, 853. (d) Jackson, J. B.; Westcott, S. L.; Hirsch, L. R.; West, J. L.; Halas, N. J. *Appl. Phys. Lett.* **2003**, *82*, 257.

(6) (a) Kottmann, J. P.; Martin, O. J. F.; Smith, D. R.; Schultz, S. *Phys. Rev. B* **2001**, *64*, 235402. (b) Sershen, S. R.; Westcott, S. L.; Halas, N. J.; West, J. L. *Appl. Phys. Lett.* **2002**, *80*, 4609. (c) Jackson, J. B.; Westcott, S. L.; Hirsch, L. R.; West, J. L.; Halas, N. J. *Appl. Phys. Lett.* **2003**, *82*, 257.

(7) (a) Murphy, C. J.; Jana, N. R. *Adv. Mater.* **2002**, *14*, 80. (b) Kim, F.; Song, J. H.; Yang, P. *J. Am. Chem. Soc.* **2002**, *124*, 14316.

(8) Westcott, S. L.; Oldenburg, S. J.; Lee, T. R.; Halas, N. J. *Chem. Phys. Lett.* **1999**, *300*, 651.

(9) Kim, S.-W.; Kim, M.; Lee, W. Y.; Hyeon, T. *J. Am. Chem. Soc.* **2002**, *124*, 7642.

(10) Li, Y.; Hong, X. M.; Collard, D. M.; El-Sayed, M. A. *Org. Lett.* **2000**, *2*, 2385.

Hollow nanostructures consisting of metals are often fabricated by depositing thin layers of metals (or their precursors) on some existing templates (e.g., silica beads and polymeric latexes), followed by calcination or wet chemical etching to remove the solid cores. As demonstrated by Halas and co-workers,[11] small gold nanoparticles (with diameter of 1−2 nm) could be adsorbed onto the surfaces of silica colloids that had been premodified with self-assembled monolayers of (3-aminopropyl)triethoxysilane. These adsorbed gold colloids could then serve as the nucleation sites for the subsequent electroless plating of gold (or other metals), leading to the formation of complete metal shells. Another method developed by Caruso and co-workers was based on the layer-by-layer adsorption of polyelectrolytes and charged gold nanoparticles to build shell-like structures around colloidal templates whose surfaces had been derivatized with appropriately charged groups.[12] More recently, silica colloids modified with (mercaptopropyl)trimethoxysilane were also used as templates to adsorb palladium acetylacetonate, which could be thermally decomposed to form a palladium shell around each template. Subsequent removal of the silica templates generated nanoshells made of palladium.[9] Although these methods are straightforward to perform and have already been demonstrated as an effective route to metal nanoshells supported on dielectric cores with controllable sizes, the resultant nanoshells are usually characterized by problems such as incomplete coverage, rough surface, nonuniformity in domain size and shell thickness, polycrystallinity, and structural fragility. It is still highly desirable to develop methods that will be able to solve some of these problems.

We have recently developed a one-step approach based on galvanic replacement reaction that was capable of generating hollow nanostructures consisting of various metals such as Au, Pd, and Pt.[13] In a typical procedure, silver nanoparticles were used as sacrificial templates to react with an aqueous HAuCl₄ solution, resulting in the formation of gold nanoshells with hollow interiors and smooth and pinhole-free surfaces, as well as homogeneous and highly crystalline walls. However, a detailed account of the morphological, structural, compositional, and spectral changes involved in the replacement reaction remains to be provided. In addition, our recent success in synthesizing silver nanostructures with well-defined shapes and surfaces (for example, nanocubes bounded by {100} crystallographic planes) also provides a number of model systems to systematically investigate the template-engaged replacement reaction on the nanometer scale.[14−18] By titrating the same amount of silver nanocubes with different volumes of the 1 mM HAuCl₄ solution, nanostructures formed at different stages of the replacement reaction have been, for the first time, fully characterized. Our results clearly showed that the template-engaged replacement reaction proceeded through two distinctive steps: (i) the formation of seamless hollow structures (with the walls made of Au−Ag alloys) via a combination of galvanic replacement (between Ag and HAuCl₄) and alloying (between Au and Ag) and (ii) the formation of hollow structures with slightly reconstructed shapes and porous walls via dealloying. Reaction temperature seemed to play the most important role in determining the final morphology of the product because the solubility product constant of AgCl and the diffusion coefficient of gold or silver atoms are both strongly dependent on this parameter.[19] Similar changes in morphology, composition, and structure were observed no matter whether silver nanocubes, nanowires, or nanospheres were used as the templates. This work has enabled us to prepare metal nanostructures with well-controlled SPR features tunable in the spectral region from 400 to 1200 nm.

2. Experimental Section

Preparation of Silver Nanostructures. Silver nanocubes were prepared using a procedure described elsewhere with some minor modifications.[14] In a typical synthesis, 5 mL of anhydrous ethylene glycol (99.8%, Aldrich, Milwaukee, WI) was heated in a 100-mL flask (ChemGlass, Vineland, NJ) at 160 °C for 1 h. A 3-mL aliquot of an ethylene glycol solution of AgNO₃ (0.25 M, 99+%, Aldrich) and poly-(vinyl pyrrolidone) (PVP, 0.19 M in terms of repeating unit, $M_w \approx$ 55 000, Aldrich) and 3 mL of an ethylene glycol solution of PVP (0.19 M) were simultaneously added to the hot ethylene glycol using a two-channel syringe pump (KDS-200, Stoelting, Wood Dale, IL) at a rate of 0.375 mL/min. The reaction mixture was then continued with heating at 160 °C for 40 min. Magnetic stirring (at a rate of ∼400 rpm) was maintained throughout the synthesis. The product was dominated by cubic nanoparticles, with a small fraction (<5%) of nanostructures with other morphologies that included, for example, rods, cubooctahedrons, tetrahedrons, and spheres.

Silver nanowires were synthesized using a polyol process similar to the one used for silver nanocubes. In a typical procedure, 3 mL of an ethylene glycol solution of AgNO₃ (0.085 M) and 3 mL of an ethylene glycol solution of PVP (0.13 M) were simultaneously injected into ethylene glycol (5 mL) that was preheated to 160 °C. For the synthesis of silver nanoparticles with a quasi-spherical shape, 0.025 g of AgNO₃ and 0.10 g of PVP were dissolved in 10 mL of ethylene glycol. This mixture was then heated at 160 °C for 1.5 h under vigorous magnetic stirring. All silver nanostructures prepared using the polyol method could form stable dispersions in water without introducing additional stabilizers.

Titration of Silver Nanostructures with a HAuCl₄ Solution. In a typical procedure, a 100-μL aliquot of the as-obtained dispersion of silver nanocubes (or 250 μL for the nanowires or spherical nanoparticles) was added to 5 mL of deionized water (E-pure, purified with cartridges from Millipore, Dubuque, IA). This diluted dispersion of

(11) (a) Oldenburg, S. J.; Averitt, R. D.; Westcott, S. L.; Halas, N. J. *Chem. Phys. Lett.* **1998**, *288*, 243. (b) Jackson, J. B.; Halas, N. J. *J. Phys. Chem. B* **2001**, *105*, 2743.

(12) (a) Caruso, F.; Spasova, M.; Salgueiriño-Maceira, V.; Liz-Marzán, L. M. *Adv. Mater.* **2001**, *13*, 1090. (b) Ji, T.; Lirtsman, V. G.; Avny, Y.; Davidov, D. *Adv. Mater.* **2001**, *13*, 1253.

(13) (a) Sun, Y.; Mayers, B. T.; Xia, Y. *Nano Lett.* **2002**, *2*, 481. (b) Sun, Y.; Xia, Y. *Anal. Chem.* **2002**, *74*, 5297. (c) Sun, Y.; Mayers, B.; Xia, Y. *Adv. Mater.* **2003**, *15*, 641. (d) Sun, Y.; Xia, Y. *Adv. Mater.* **2004**, *16*, 264. (e) Métraux, G. S.; Cao, Y. C.; Jin, R.; Mirkin, C. A. *Nano Letters* **2003**, *3*, 519.

(14) Nanocubes: Sun, Y.; Xia, Y. *Science* **2002**, *298*, 2176.

(15) Triangular nanoplates: (a) Jin, R.; Cao, Y.; Mirkin, C. A.; Kelly, K. L.; Schatz, G. C.; Zheng, J. G. *Science* **2001**, *294*, 1901. (b) Jin, R.; Cao, Y. C.; Hao, E. C.; Metraux, G. S.; Schatz, G. C.; Mirkin, C. A. *Nature* **2003**, *425*, 487. (c) Chen, S.; Carroll, D. L. *Nano Lett.* **2002**, *2*, 1003. (d) Pastoriza-Santos, I.; Liz-Marzán, L. M. *Nano Lett.* **2002**, *2*, 903. (e) Maillard, M.; Giorgio, S.; Pileni, M.-P. *Adv. Mater.* **2002**, *14*, 1084. (f) Sun, Y.; Xia, Y. *Adv. Mater.* **2003**, *15*, 695. (g) Sun, Y.; Mayers, B.; Xia, Y. *Nano Lett.* **2003**, *3*, 675.

(16) Circular nanodisks: (a) Chen, S.; Fan, Z.; Carroll, D. L. *J. Phys. Chem. B* **2002**, *106*, 10777. (b) Yener, D. O.; Sindel, J.; Randall, C. A.; Adair, J. H. *Langmuir* **2002**, *18*, 8692. (c) Sun, Y.; Xia, Y. *Analyst* **2003**, *128*, 686.

(17) Nanorods: (a) Jana, N. R.; Gearheart, L.; Murphy, C. J. *Adv. Mater.* **2001**, *13*, 1389. (b) Jana, N. R.; Gearheart, L.; Murphy, C. J. *J. Phys. Chem. B* **2001**, *105*, 4065. (c) Jana, N. R.; Gearheart, L.; Murphy, C. J. *Chem. Commun.* **2001**, 617. (d) Yu, Y.-Y.; Chang, S.-S.; Lee, C.-L.; Wang, C. R. C. *J. Phys. Chem. B* **1997**, *101*, 6661.

(18) Nanowires: (a) Xia, Y.; Yang, P.; Sun, Y.; Wu, Y.; Mayers, B.; Gates, B.; Yin, Y.; Kim, F.; Yan, H. *Adv. Mater.* **2003**, *15*, 353. (b) Sun, Y.; Mayers, B.; Herricks, T.; Xia, Y. *Nano Lett.* **2003**, *3*, 955. (c) Sun, Y.; Yin, Y.; Mayers, B. T.; Herricks, T.; Xia, Y. *Chem. Mater.* **2002**, *14*, 4736. (d) Sun, Y.; Gates, B.; Mayers, B.; Xia, Y. *Nano Lett.* **2002**, *2*, 165. (e) Sun, Y.; Xia, Y. *Adv. Mater.* **2002**, *14*, 833.

(19) Dick, K.; Dhanasekaran, T.; Zhang, Z.; Meisel, D. *J. Am. Chem. Soc.* **2002**, *124*, 2312.

silver nanocubes was then refluxed for 10 min before a specific volume of 1 mM HAuCl₄ (99.9%, Aldrich) aqueous solution was added dropwise. The mixture was refluxed for another 20 min until its color became stable. Vigorous magnetic stirring was maintained in the entire process. As the solution was cooled to room temperature, white solid—AgCl precipitate—was found to settle at the bottom of the container. The AgCl solid could be removed by dissolving with a saturated solution of NaCl. In this case, NaCl powders (99.9%, Fisher, Fairlawn, NJ) were added to the aqueous dispersion of product until it was saturated with NaCl. The solution was then transferred into a tube and centrifuged at 10 000 rpm for 15 min. The supernatant containing the dissolved AgCl could be easily removed using a pipet. The solid was rinsed with water and centrifuged six more times and finally dispersed with water for further characterization and usage.
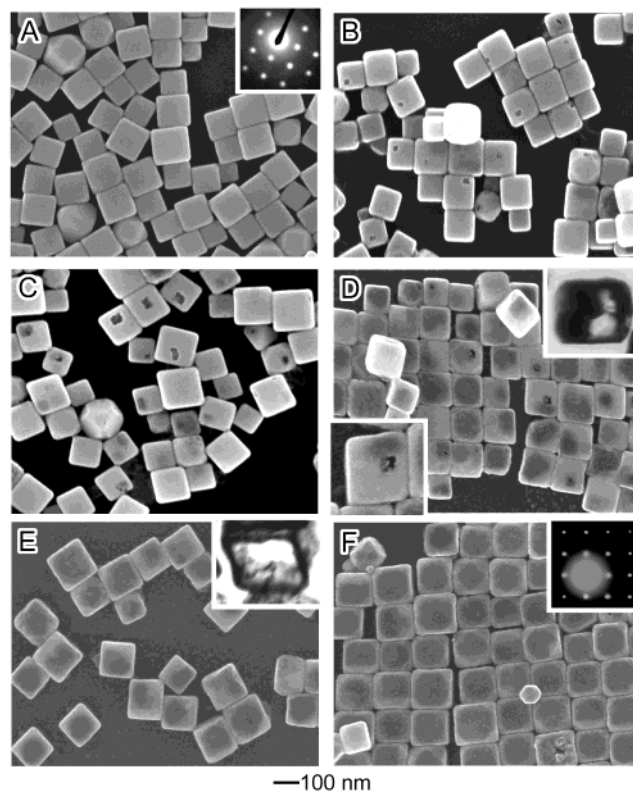
Instrumentation. The samples for scanning electron microscopy (SEM) and transmission electron microscopy (TEM) studies were prepared by placing small drops of the dispersions of metal nanostructures on silicon substrates (Silicon Valley Microelectronics, San Jose, CA) and copper grids (Ted Pella, Redding, CA), respectively. The samples were allowed to dry at room temperature in a fume hood. In the preparation of microtomed samples, the dried nanostructures were dispersed in the Spurr's epoxy with a low viscosity (Polysciences, Warrington, PA) and then polymerized at 70 °C for 24 h. The microtome (Reichert/Jung Ultra-cut E, Leica, Arcadia, CA) equipped with a diamond knife was used to cut the cured epoxy resin into slices with thicknesses of less than 100 nm. These slices were placed on copper grids for TEM observations. The SEM images were obtained using a field-emission microscope (Sirion XL, FEI, Hillsboro, OR) operated at 15 kV. Energy-dispersive X-ray (EDX) measurements were conducted with the EDAX system attached to the same microscope. TEM images and electron diffraction patterns were taken using a JEOL microscope (1200EX II, Peabody, MA) operated at 80 kV. The percentages of gold and silver in the nanostructures were analyzed using the atomic emission spectrophotometer (Thermo Jarrell Ash Corp., Franklin, MA) equipped with a Jarrell Ash 955 inductively coupled plasma system. The emission lines at 328.0 and 242.8 nm were used to measure the contents of silver and gold, respectively. All UV—visible—near-IR spectra were recorded at room temperature on a Cary 5E (Varian, Walnut Creek, CA) spectrometer using quartz cuvettes with an optical path of 1 cm.

3. Results Obtained for Silver Nanocubes

Galvanic replacement reaction has been demonstrated as a general and effective means for preparing metallic nanostructures (e.g., thin films) by consuming the more reactive component.[20] We have focused on silver nanocubes because this class of nanostructures provides a model system with monodispersed size and well-defined facets. Since the standard reduction potential of $AuCl_4^-/Au$ pair (0.99 V vs standard hydrogen electrode, SHE) is higher than that of the Ag^+/Ag pair (0.80 V vs SHE), silver would be oxidized into Ag^+ when silver nanostructures and HAuCl₄ are mixed in an aqueous medium:

$$3Ag(s) + AuCl_4^-(aq) \rightarrow Au(s) + 3Ag^+(aq) + 4Cl^-(aq) \tag{1}$$
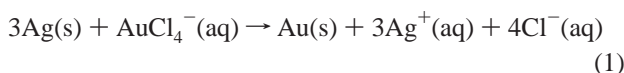
Morphological and Structural Changes Involved in the Reaction. Both SEM and TEM were used to follow the morphological and structural changes involved in various stages of the replacement reaction between silver nanocubes and

(20) (a) Lin, W.; Warren, T. H.; Nuzzo, R. G.; Girolami, G. S. *J. Am. Chem. Soc.* **1993**, *115*, 11644. (b) Poter, L. A., Jr.; Choi, H. C.; Ribbe, A. E.; Buriak, J. M. *Nano Lett.* **2002**, *2*, 1067.

Figure 1. Formation of Au—Ag nanoboxes through a combination of galvanic replacement reaction (between Ag and HAuCl₄) and alloying (between Au and Ag). The SEM images were taken from silver nanocubes (A) before and (B—F) after they had reacted with different volumes of 1 mM HAuCl₄ solution: (B) 0.05, (C) 0.10, (D) 0.30, (E) 0.50, and (F) 0.75 mL. The formation of hollow structures was confirmed by TEM studies on the microtomed samples (the insets at the upper right-hand corners of panels D and E). The formation of slightly truncated corners for the nanoboxes shown in F implies the initiation of dealloying.

HAuCl₄. Figures 1 and 2 show SEM images of silver nanocubes (all started with the same amount) before and after they had reacted with different volumes of 1 mM HAuCl₄ at 100 °C. Figure 1A gives a typical SEM image of the silver nanocubes, indicating the monodispersity that could be achieved using the modified polyol process. These silver nanocubes were characterized by smooth surfaces and a mean edge length around 111 nm (with a standard deviation of 13 nm). The inset provides an electron diffraction pattern that was obtained by aligning the electron beam perpendicular to one of the square faces of a cube. The square symmetry displayed by the pattern indicates that each silver nanocube was a single-crystal bounded by {100} facets. After the silver nanocubes had reacted with a very small amount (i.e., 0.05 mL) of HAuCl₄ solution, a small hole was formed at a specific site of the surface, indicating that the replacement reaction was initiated locally rather than over the entire surface. As shown in Figure 1B, the holes can be clearly observed as black spots on the surfaces of some cubes. A statistical analysis on hundreds of cubes indicated that only about one-sixth of the cubes showed holes on their surfaces when viewed under SEM. This observation suggested that only one hole was formed on each nanocube because each cube was enclosed by six equivalent, square faces and each face should have the same probability to be oriented toward the observer. The newly formed surfaces containing holes should represent the most active sites for further replacement reaction. The
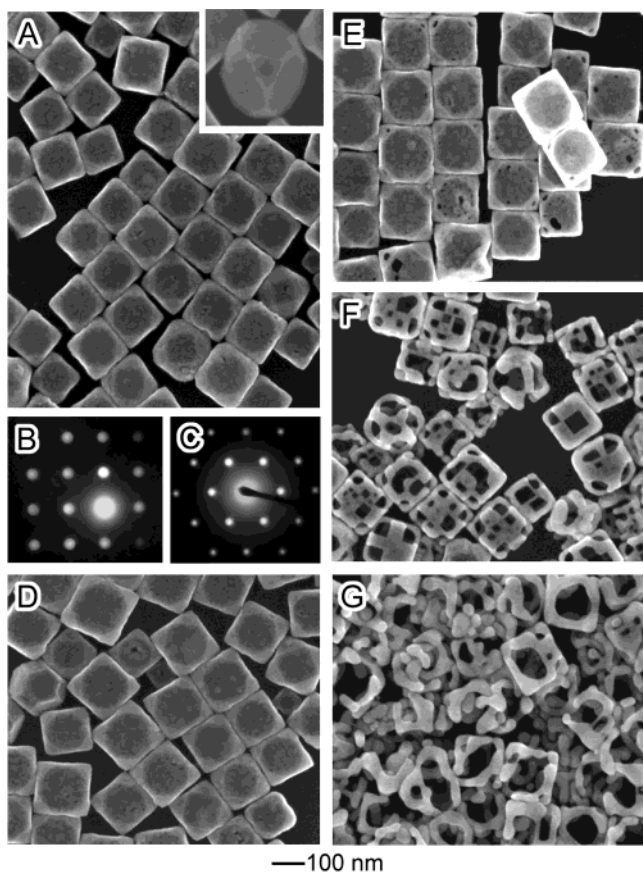
Figure 2. Dealloying of Au−Ag nanoboxes as the volume of 1 mM HAuCl₄ solution was further increased. The SEM images were taken from the same batch of silver nanocubes after they had reacted with different volumes of 1 mM HAuCl₄ solution: (A) 1.00, (D) 1.50, (E) 2.00, (F) 2.25, and (G) 2.50 mL. (B, C) Electron diffraction patterns taken from individual Au−Ag nanoboxes by aligning electron beam perpendicular to one of the octagonal or triangular faces, respectively.

dimensions of each cube exhibited no apparent change in the initial stage of this reaction, indicating that the gold atoms were deposited on the surface of each cube as a very thin (most likely, incomplete) shell. As a result, the replacement reaction could be continued to generate larger holes (Figure 1C). The coating of gold would become thicker as more gold atoms were generated from the replacement reaction. Once the thickness of the gold shell had reached a critical value (~1 nm), the size of each hole would start to shrink due to a combination of volume diffusion, surface diffusion, and/or dissolution and deposition promoted at 100 °C.[21] As shown in Figure 1D, the opening on the surface of each cube was, indeed, reduced in area as compared to those shown in Figure 1C. The inset in the lower left corner of Figure 1D gives the enlarged image of an individual cube, clearly revealing an increase in edge roughness for the hole. The formation of extruded structures toward the center of the hole implied that the shrinkage of the hole might be dominated by a mass diffusion process. In addition, the TEM image of a microtomed sample (shown as an inset at the upper right-hand corner) shows that the nanostructure formed at this stage was a partially hollow cube.
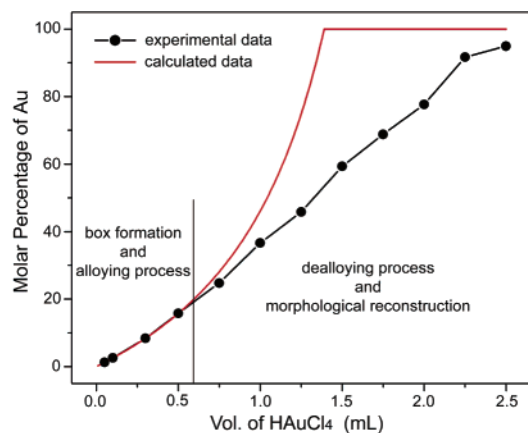
If the volume of the HAuCl₄ solution was increased, the void within each cube would increase further to form cubic nanoboxes with uniform walls, as confirmed by the TEM image taken

(21) Sieradzki, K. *J. Electrochem. Soc.* **1993**, *140*, 2868.

from a microtomed nanobox (see the inset of Figure 1E). Note that all holes had now disappeared to generate nanoboxes with smooth, seamless surfaces. When the volume of the HAuCl₄ solution was increased to 0.75 mL (Figure 1F), all nanocubes had been transformed into pinhole-free nanoboxes whose mean edge length was slightly increased to 117 nm as compared with that of the original silver nanocubes. This result indicated that the gold atoms were deposited on the exterior surface of each silver nanocube. The electron diffraction pattern (shown as the inset of Figure 1F) that was recorded by directing the electron beam perpendicular to one of the square surfaces displayed the same symmetry as that of a silver nanocube. This observation implies the existence of an epitaxial relationship between the walls of each nanobox and the surfaces of the silver nanocube in the replacement reaction. Note that the corners of some nanoboxes were slightly truncated at this point, indicating the initiation of dealloying.

As the dealloying process was continued, the newly formed triangular faces were further enlarged in area to cause more significant truncation for the corners of each nanobox. Figure 2A shows a typical SEM image of such truncated nanoboxes, and each of them was bounded by two sets of facets: eight triangular ones and six octagonal ones. The inset shows the SEM image of a truncated nanobox sitting on the silicon substrate against one of its triangular facets. The crystallinity of these truncated nanoboxes was examined by electron diffraction. Parts B and C of Figure 2 show the electron diffraction patterns recorded from two nanoboxes sitting on the TEM grids against one of their octagonal and triangular facets, respectively. These patterns indicated that each truncated nanobox was a single crystal, with the octagonal facets corresponding to {100} crystallographic planes and the triangular ones to {111} planes. As the volume of the 1 mM HAuCl₄ solution was increased, small pinholes of 1−5 nm in cross-section started to appear in the walls of truncated nanoboxes (see Figure 2D). The densities of the pinholes and their dimensions were both increased as dealloying was allowed to proceed (Figure 2E). Once the dimensions of these pinholes had reached a critical value, they tended to coalesce into larger pores with sizes ranging from 20 to 60 nm (Figure 2F). The truncated corners bounded by {111} facets were also replaced with large pores. As confined by symmetry, most pores clearly exhibited a square profile. Our electron diffraction studies implied that these boxes with pores in their surfaces (cubic nanocages) were also single crystals bounded by {100} planes. These nanocages would collapse into gold fragments (see Figure 2G for a typical example) after 2.5 mL of 1 mM HAuCl₄ solution had been added to the dispersion of silver nanocubes. To our knowledge, this work represents the first detailed study with regard to the dealloying of single crystalline nanostructures of a Au−Ag alloy textured by {100} facets.
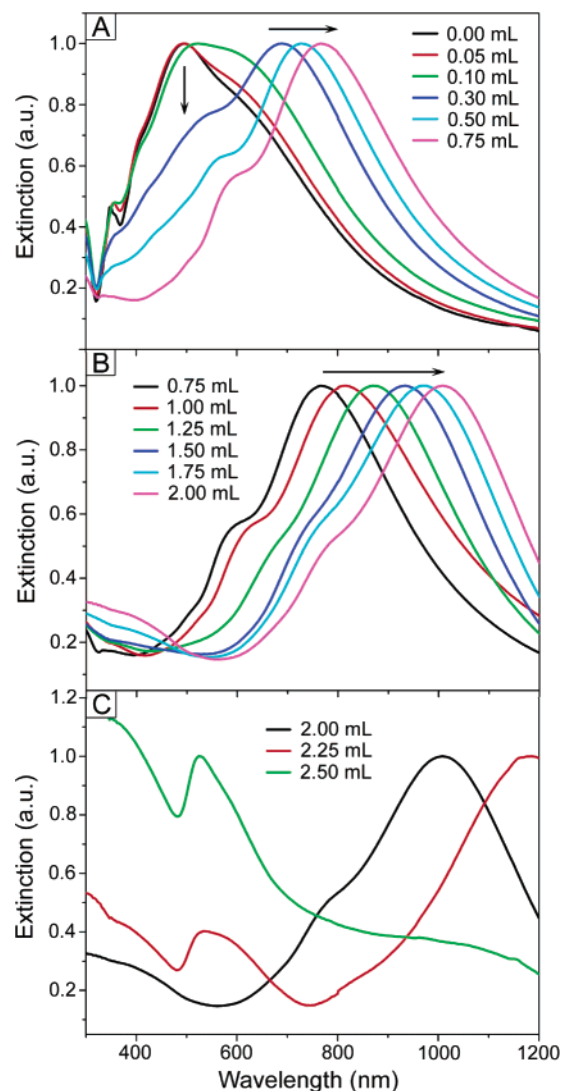
Compositional Changes Associated with the Replacement Reaction. We first used EDX spectroscopy to determine the composition of seamless nanoboxes (shown in Figure 2A) that had been purified by removing the AgCl solid with a super-saturated NaCl solution. The spectrum displayed strong peaks for both gold and silver, while no signal for Cl was detected. The absence of Cl in the purified product was also confirmed by atomic emission spectroscopic analysis. Combining with the single crystallinity revealed by electron diffraction and high-

Figure 3. Relationship between the molar percentage of Au in the alloyed hollow nanostructures and the volume of the 1 mM HAuCl$_4$ solution that had been added to react with silver nanocubes.

resolution TEM imaging (as shown in Figure 4 of ref 13a), it is conclusive that these nanoboxes were composed of a homogeneous Au−Ag alloy rather than a heterogeneous or mosaic structure. We have also used atomic emission spectroscopy to precisely analyze the percentages of gold and silver in the hollow nanostructures that were prepared by adding different volumes of 1 mM HAuCl$_4$ solution to the same amount of silver nanocubes. The inductively coupled plasma could directly atomize the metal nanostructures because its flame could reach a temperature as high as 9000 K.[22] The molar percentages of gold in a set of products are shown in Figure 3. This result indicates that more gold was generated as more HAuCl$_4$ was added to the dispersion of silver nanocubes. According to the stoichiometric relationship shown in eq 1, the calculated percentage of gold in the hollow Au−Ag nanostructure is also plotted in Figure 3 as a function of the volume of the HAuCl$_4$ solution (the curve in red). The sharp change at 1.3 mL implies that this amount of the 1 mM HAuCl$_4$ solution could completely oxidize the silver nanocubes into silver ions if they were able to react with efficiency close to 100%. However, experimental data indicate that much more HAuCl$_4$ solution was required to reach this point, and this volume could be as high as 2.5 mL. We ascribed this discrepancy to the dealloying process that seemed to need HAuCl$_4$ with much higher chemical potentials to selectively dissolve the silver atoms. When the volume of HAuCl$_4$ solution was lower than 0.6 mL, the experimental data matched well with the calculated curve, indicating that HAuCl$_4$ mainly reacted with the pure silver in this region. The analyses were consistent with the results of microscopic studies shown in Figures 1 and 2. In the early stage, HAuCl$_4$ only reacted with the pure silver templates rather than on the Au−Ag alloyed surfaces because pure silver is more reactive than the alloyed silver. This reaction resulted in the formation of nanoboxes consisting of Au−Ag alloys. After the boxes had been formed, addition of more HAuCl$_4$ would dealloy the boxes along with morphological reconstructions. The molar percentage of Au reached 95% when the volume of the HAuCl$_4$ solution was increased to 2.5 mL, confirming that the fragments (as shown in Figure 2G) obtained as the final product of the replacement reaction were essentially made of pure gold.

(22) *Inductively Coupled Plasma Emission Spectroscopy*, Boumans, P. W. J. M., Ed.; John Wiley & Sons: New York, 1987; Vol. 90, Part 1, pp 69−99.

Figure 4. UV−visible−near-IR extinction spectra of aqueous dispersions of silver nanocubes (all in the same amount) before and after reacting with different volumes (as indicated on each plate) of 1 mM HAuCl$_4$ aqueous solution. On the basis of spectral changes, the replacement reaction could also be separated into three stages: (A) formation of Au−Ag alloyed nanoboxes; (B) dealloying of the Au−Ag boxes; and (C) fragmentation of the boxes into discrete nanostructures. All spectra are normalized against the intensities of their strongest peaks.

Spectral Evolution Involved in the Replacement Reaction. We could also conveniently monitor the galvanic replacement reaction between silver nanocubes and the HAuCl$_4$ solution by spectroscopic means because nanostructures made of gold and/ or silver often exhibit distinctive SPR peaks in the UV−visible− near-IR region that are strongly dependent on their shape and structure (solid vs hollow).[6] Figure 4 shows the extinction spectra recorded from aqueous dispersions of silver nanocubes (in the same amount for all measurements) after they had reacted with different volumes of 1 mM HAuCl$_4$ solution at 100 °C. The spectral changes shown in Figure 4A were consistent with the formation of seamless nanoboxes with their walls composed of homogeneous Au−Ag alloys. In this case, the silver nanocubes exhibited a major peak at 495 nm, together with three shoulder peaks at 350, 400, and 600 nm, respectively. When a small volume (between 0.05 and 0.10 mL) of HAuCl$_4$ solution was added to the dispersion of silver nanocubes, we observed almost no change for the main peak and the extinction bands at
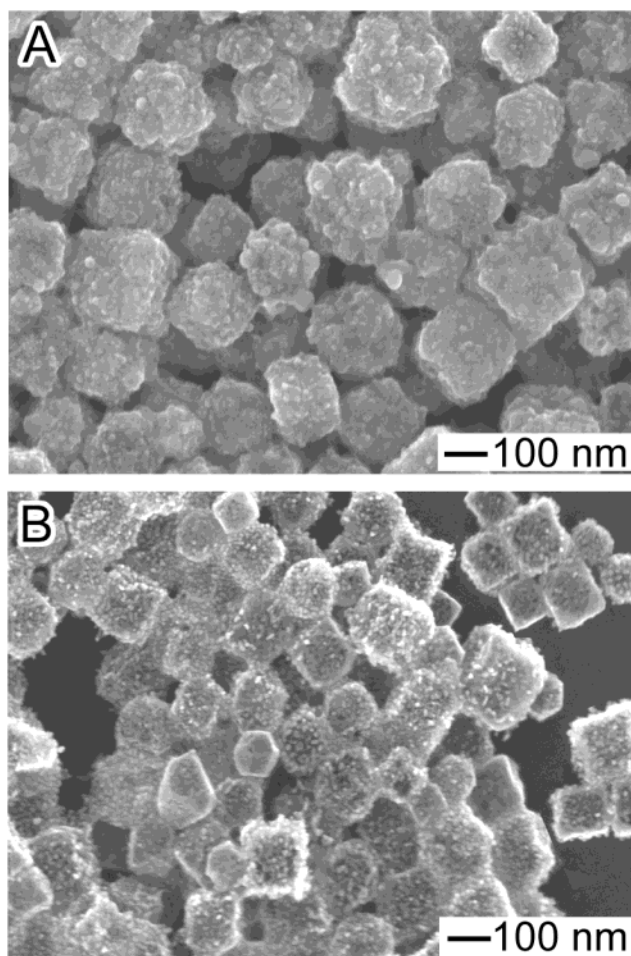
shorter wavelengths, while the extinction at longer wavelengths (>520 nm) displayed a significant increase. This spectral change could be attributed to the deposition of thin gold layers on the surfaces of silver templates, which were further transformed into thin shells of Au−Ag alloys. The peak at 495 nm for silver cubes continued to decrease in intensity as more aqueous HAuCl₄ solution was added to the reaction system. This peak disappeared after 0.75 mL of 1 mM HAuCl₄ solution had been introduced, indicating the formation of nanoboxes enclosed by Au−Ag alloyed walls. At the same time, the extinction peaks at longer wavelengths were red-shifted to 770 nm. This shift in peak position might be caused by the increase in void size and the reduction in wall thickness for the boxes.[23]

The spectral changes involved in the dealloying process of Au−Ag nanoboxes are shown in Figure 4B,C. It is worth noting that the extinction peak could be further red-shifted to 1180 nm if 2.25 mL of HAuCl₄ solution was added to the reaction mixture. In this case, the peak shift was believed to be related to the formation of pinholes with increasing sizes in the walls. The reduction in wall thickness, which played an important role in determining the SPR features,[23] might also be involved in the dealloying process. Due to their high absorption coefficient in the near-IR region (800−1200 nm, the transparent window of soft tissues), the nanoscale boxes and cages described here might find use in a range of medical applications such as photothermally triggered drug releasing, photothermal cancer therapy, and contrast-enhanced imaging.[24] When the silver nanocubes were reacted with 2.50 mL of 1 mM HAuCl₄ solution, the peak in the near-IR region disappeared, indicating that the nanoboxes had collapsed into small fragments (or solid gold nanoparticles) and the extinction peak was blue-shifted back to ~525 nm (the green curve in Figure 4C).

Influence of Temperature on the Replacement Process. The reaction temperature was found to play a critical role in forming seamless nanoboxes with smooth and uniform walls. As shown in Figure 5A, the silver nanocubes were transformed into structures with rough surfaces and irregular sizes when the reaction was performed under conditions similar to those used in Figure 1F except that the temperature was reduced from 100 to 20 °C. The striking difference in morphology observed here can be attributed to two major factors: (i) AgCl solid has a smaller solubility product constant (k_{sp}) at room temperature, which might lead to the simultaneous formation of AgCl precipitation during the replacement reaction; (ii) the inter-diffusion rate between Ag and Au is also greatly reduced at low temperature, which might result in a product with hetero-geneous structure rather than a homogeneous alloy. Our EDX analysis of the product indicated that the rough surfaces were mainly composed of Au and AgCl nanocrystals. Both the polycrystallinity of gold and the contamination of AgCl nano-crystals caused the resultant particle to become rougher in surface and larger in size. This result implied that the simul-taneous formation of solid AgCl and gold might disrupt the epitaxial deposition of gold atoms on the surface of a silver template. The slowed interdiffusion between Ag and Au might also further hinder the epitaxial deposition of gold.

(23) Westcott, S. L.; Oldenburg, S. J.; Lee, T. R.; Halas, N. J. *Chem. Phys. Lett.* **1999**, *300*, 651.
(24) (a) Sershen, S. R.; Westcott, S. L.; Halas, N. J.; West, J. L. *J. Biomed. Mater. Res.* **2000**, *51*, 293. (b) Hirsch, L. R.; Stafford, R. J.; Bankson, J. A.; Sershen, S. R.; Rivera, B.; Price, R. E.; Hazle, J. D.; Halas, N. J.; West, J. L. *Proc. Natl. Acad. Sci. U.S.A.* **2003**, *100*, 13549.

Figure 5. (A) SEM image of the product obtained by reacting silver nanocubes with 0.75 mL of 1 mM HAuCl₄ solution at room temperature. Except for temperature, all other conditions were similar to those used in Figure 1F. (B) SEM image of Au−Ag alloyed nanoboxes (see Figure 1F for an SEM image) after they had reacted with some additional amount of aqueous HAuCl₄ solution at room temperature.
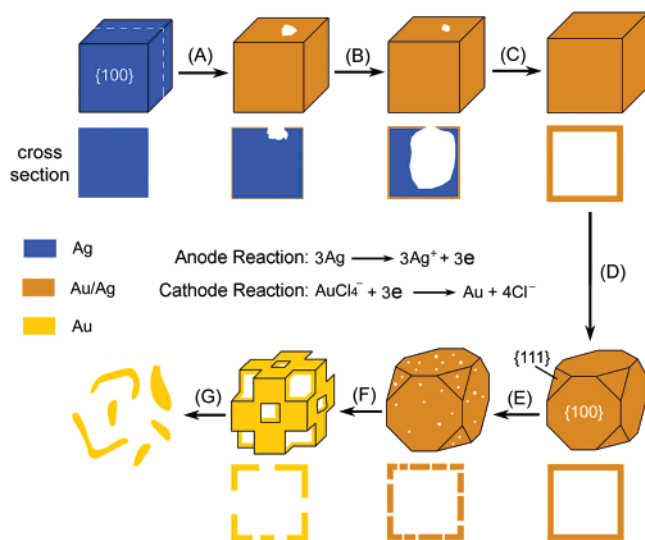
The dealloying process of Au−Ag alloyed nanoboxes was also strongly dependent on the temperature. We demonstrated this point by reacting the nanoboxes shown in Figure 1F with some additional HAuCl₄ solution (0.25 mL) at different tem-peratures. At 100 °C, nanoboxes with smooth surfaces were formed, with a quality similar to that of the product shown in Figure 2A. At room temperature, however, the nanoboxes were transformed into porous structures covered with small particles, with a typical SEM image shown in Figure 5B. The formation of pores in the walls indicated the silver atoms contained in the alloy had been dissolved with HAuCl₄. This observation suggested that the galvanic replacement reaction involved in the dealloying process was strongly independent of temperature. On the other hand, the rate of Ostwald ripening, which was believed to be responsible for morphological reconstruction and surface smoothening, could also decrease when the temperature was reduced.

4. Discussion

With silver nanocubes as an example, Figure 6 summarizes all major steps involved in the galvanic replacement process that is performed at 100 °C. After the HAuCl₄ solution has been added to the dispersion of silver nanocubes bounded by {100}

Figure 6. Schematic illustration summarizing all morphological and structural changes involved in the galvanic replacement reaction between a silver nanocube and an aqueous $HAuCl_4$ solution. The major steps include the following: (A) initiation of replacement reaction at a specific spot with relatively high surface energy; (B) continuation of the replacement reaction between Ag and $HAuCl_4$ and the formation of a partially hollow nanostructure; (C) formation of nanoboxes with a uniform, smooth, homogeneous wall composed of Au−Ag alloy; (D) initiation of dealloying and morphological reconstruction of the Au−Ag nanobox; (E, F) continuation of dealloying, together with the formation of pores in the wall; and (G) fragmentation of the porous Au nanobox. The cross-sectional views correspond to the plane along dashed lines.

facets, the replacement reaction will start from the sites with relatively high surface energies (typical examples include steps, point defects, and stacking faults).[25] Once the reaction has started on the active site of each nanocube, the silver will start to dissolve and a hole will be generated on one of its six faces. The reaction is like a corrosion process, with silver being oxidized at the anode. The released electrons can easily migrate to the surface of the cube and be used to reduce $AuCl_4^-$ into Au atoms (cathode reaction). The elemental gold generated in the replacement reaction tends to be deposited on the surface of each template because of a good matching between the crystalline structures (both gold and silver are face-centered cubic) and lattice constants (4.0786 and 4.0862 Å for gold and silver, respectively). The epitaxial deposition will lead to the formation of a thin, incomplete layer of gold (step A), which can prevent the underneath silver from reacting with $HAuCl_4$. As a result, the hole will continue to serve as an active site for subsequent reaction. At the same time, such an opening on the surface allows all the species (e.g., $AuCl_4^-$, Ag^+, Cl^-, and Au) to continuously diffuse in and out of the hole. The dissolution of silver transforms each silver nanocube into a structure characterized by a hollow interior (step B). The generated gold atoms continue to grow on the outer surface of the template and gradually reduce the area of opening via various mass diffusion processes.

When the concentration of $HAuCl_4$ is high enough, the void size inside the template will be enlarged to its maximum size and the hole on its surface will disappear, leading to the formation of a boxlike structure with uniform and homogeneous walls (step C). Along with the replacement reaction between the silver template and $HAuCl_4$ (steps A, B, and C), alloying

also occurs between the deposited gold layer and the underlying silver surface because the diffusion rates of silver and gold atoms are relatively high at 100 °C.[19] As a matter of fact, silver and gold tend to form a nearly ideal solid solution because the homogeneous Au−Ag alloy will be more stable than either pure Au or Ag.[26] In this case, the composition profile of the Au−Ag alloyed wall should evolve with time according to Fick's second law. The relevant solution for the interdiffusing interface with mutually soluble components can be expressed as[27]

$$C(x,t) = 0.5 + 0.5erf\{x/[2(Dt)^{1/2}]\} \qquad (2)$$

Here, D is the interdiffusion coefficient, and C is the atomic fraction of gold as a function of time (t) and distance (x) separated from the interface. D is strongly dependent on the temperature and film thickness. Its magnitude can be significantly increased as the temperature is raised and the thickness of gold layer is reduced.[19,28] Miesel and co-workers had investigated the spontaneous alloying process of Au−Ag core−shell nanoparticles with different sizes.[29] Their results suggested that the D was on the order of 10^{-24} m^2 s^{-1} at room temperature when 2.5 nm Au core particles were coated with 1-nm Ag layers. On the basis of the Arrhenius equation

$$D = D_0 \exp(-\Delta H_a/kT) \qquad (3)$$

the value of D is estimated to be on the order of 10^{-19} m^2 s^{-1} when the temperature is increased to 100 °C. In this case, the activation enthalpy, ΔH_a, is taken as 1.58 eV.[30] In our experiments, the gold layers formed at the early stages (steps A, B, and C) were thinner than 2.5 nm. Therefore, it is reasonable to assume that the interdiffusion coefficient is around 10^{-19} m^2 s^{-1} in the formation of Au−Ag alloy walls. According to eq 2, the gold layer should contain at least 10% silver even though the nanobox is only annealed at 100 °C for 20 s. As the annealing time is prolonged, a more homogeneous wall with a high percentage of Ag should be formed.

If more $HAuCl_4$ is added to the reaction system, the silver atoms in the Au−Ag nanoboxes will be selectively removed. In this so-called *dealloying process*,[31] numerous lattice vacancies will be formed because only one gold atom can be generated at the expense of three silver atoms, according to the stoichiometric relationship shown in eq 1. These defects can generate negative curvatures for the solid walls and thus cause the interfacial area and the surface energy to increase.[21] To release these lattice vacancies, the nanobox will reconstruct its morphology via Ostwald ripening.[32] As a result, each corner of the box will be truncated to form new faces bounded by a {111} crystallographic plane (step D). Such a morphological change saves the total surface energy in two ways: (i) by reducing the total surface area by replacing three {100} planes of each corner with one {111} plane and (ii) by reducing the surface energy per

(25) Wang, Z. L.; Ahmad, T. S.; El-Sayed, M. A. *Surf. Sci.* **1997**, *380*, 302.

(26) Shi, H.; Zhang, L.; Cai, W. *J. Appl. Phys.* **2000**, *87*, 1572.
(27) Porter, D. A.; Easterling, K. E. *PhaseTtransformation in Metals and Alloys*, 2nd ed.; Chapman & Hall: London, 1992.
(28) (a) Wonnell, S. K.; Delaye, J. M.; Bibolé, M.; Limoge, Y. *J. Appl. Phys.* **1992**, *72*, 5195. (b) Ding, Y.; Erlebacher, J. *J. Am. Chem. Soc.* **2003**, *125*, 7772.
(29) Shibata, T.; Bunker, B. A.; Zhang, Z.; Meisel, D.; Vardeman, C. F., II; Gezelter, J. D. *J. Am. Chem. Soc.* **2002**, *124*, 11989.
(30) Bukaluk, A. *Appl. Surf. Sci.* **2001**, *175−176*, 790.
(31) Erlebacher, J.; Aziz, M. J.; Karma, A.; Dimitrov, N.; Sieradzki, K. *Nature* **2001**, *410*, 450.
(32) Roosen, A. R.; Carter, W. C. *Physica A* **1998**, *261*, 232.

unit area by replacing the less stable {100} planes with the more stable {111} ones.[33] As more silver atoms in the truncated box are dissolved by $AuCl_4^-$ ions, more lattice vacancies will be formed. In this case, the Ostwald ripening process cannot reconstruct the box to form a continuous box with thinner walls because such structures are not stable at 100 °C. To this end, the lattice vacancies will start to coalesce and generate pinholes in the wall (step E). Further dealloying will enlarge the lateral dimensions of the pinholes (step F). It is interesting to note that these pinholes tend to form square profiles once their dimensions have reached a critical value (∼20 nm). The specific shape of these pores might be related to the square arrangement of atoms on each wall where the surface is mainly bounded by {100} crystallographic planes. Complete dealloying will cause the porous nanobox (or nanocage) to collapse into small fragments of pure gold (step G).

The formation of AgCl solid has to be considered because the crystallization of metallic surfaces might be influenced by the simultaneous precipitation of AgCl. The solubility product (k_{sp}) of AgCl is ∼1.8×10^{-10} in water at 20 °C. When the temperature (T) is raised, it will increase accordingly because the dissolution process has a positive enthalpy (ΔH_0). When the reaction is performed at 100 °C, the solubility product of AgCl can reach a value of ∼1.2×10^{-6} as predicted by

$$\ln \frac{k_{sp}^2}{k_{sp}^1} = -\frac{\Delta H_0}{R}\left(\frac{1}{T_2} - \frac{1}{T_1}\right)$$
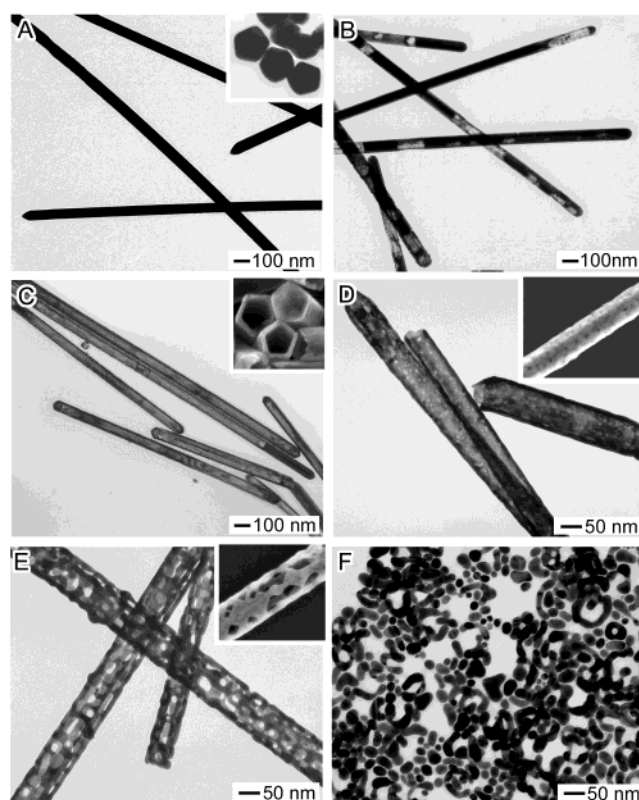
where R is the gas constant and $\Delta H_0 = 65.57$ kJ/mol.[34] In our synthesis, the maximum concentrations of chloride and silver ions in the final reaction solution were ∼5.6×10^{-4} and ∼1.33×10^{-3} M, respectively. The product of these two concentrations was only 7.4×10^{-7}, a value that fell between the solubility products of AgCl at 20 and 100 °C. As a result, no AgCl precipitate should be formed in the medium when the reaction is carried out at 100 °C. White solid appeared at the bottom of the reactor when the reaction mixture was cooled to room temperature, indicating the formation of AgCl precipitate. The separation of gold deposition and AgCl precipitation into two steps helps to prevent the gold shells from being contaminated by AgCl. It also helps to maintain the epitaxial growth of gold shells on silver templates and thus allows for the formation of single crystalline Au−Ag shells. If necessary, the AgCl precipitate can be easily dissolved with a saturated NaCl solution through the coordination reaction[35]

$$AgCl(s) + 3Cl^-(aq) \rightarrow AgCl_4^-(aq) \tag{4}$$
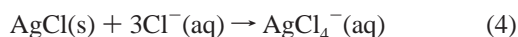
The metal nanostructures with hollow interiors can be readily collected as a pure sample through centrifugation and then redispersed in water for further application.

5. Extension to Silver Nanowires and Nanospheres

Different from silver nanocubes (which are single crystals), nanowires and nanospheres are often polycrystalline structures characterized by various degrees of twinning and more complex sets of facets. It will be interesting to see if the mechanism

(33) Wang, Z. L. *J. Phys. Chem. B* **2000**, *104*, 1153.
(34) *CRC Handbook of Chemistry and Physics*, 62nd ed.; Weast, R., Ed.; CRC Press: Boca Raton, FL, 1981.
(35) Lampre, I.; Pernot, P.; Mostafavi, M. *J. Phys. Chem. B* **2000**, *104*, 6233.

Figure 7. TEM images taken from silver nanowires (A) before and (B−F) after they had reacted with different volumes of 1 mM HAuCl₄ solution: (B) 0.3, (C) 0.6, (D) 1.5, (E) 2.3, and (F) 3.0 mL. The inset of A shows TEM image taken from the microtomed sample of silver nanowires. The insets of C−E are SEM images of the corresponding products.

sketched in Figure 6 can be extended to describe the galvanic replacement reactions between these nanostructures (commonly obtained via a variety of synthetic routes) and HAuCl₄ solutions.

Galvanic Replacement Reaction between Silver Nanowires and HAuCl₄. Silver nanowires represent another class of nanostructures that could be readily synthesized using the polyol method. Such a nanowire had a pentagonal cross-section (as shown in the inset of Figure 7A), five straight side edges parallel to its long axis, five flat side surfaces bounded by {100} facets, 10 {111} end facets, and a twinned crystalline structure of 5-fold symmetry.[18b] We have also investigated the reaction between these silver nanowires and various volumes of the 1 mM HAuCl₄ solution. TEM images of the resultant nanostructures are shown in Figure 7. When 0.3 mL of HAuCl₄ was used (Figure 7B), each silver nanowire developed interior cavities (i.e., tubular strips). Once the volume of the HAuCl₄ solution had been increased to 0.6 mL (Figure 7C), all the silver nanowires were transformed into nanotubes with smooth and uniform sheaths. Note that the nanotubes essentially inherited all the morphological features associated with silver nanowires. As shown in the inset, each tube also had a pentagonal cross-section, five straight side edges, and five flat side surfaces. Electron diffraction patterns taken from individual nanotubes were essentially the same as those of silver nanowires. These observations further confirmed that the elemental gold generated from the replacement reaction was epitaxially deposited on the surfaces of silver templates. Dealloying of these Au−Ag alloyed nanotubes also led to the formation of pinholes in their surfaces (Figure 7D,E). The pore size was dependent on the volume of
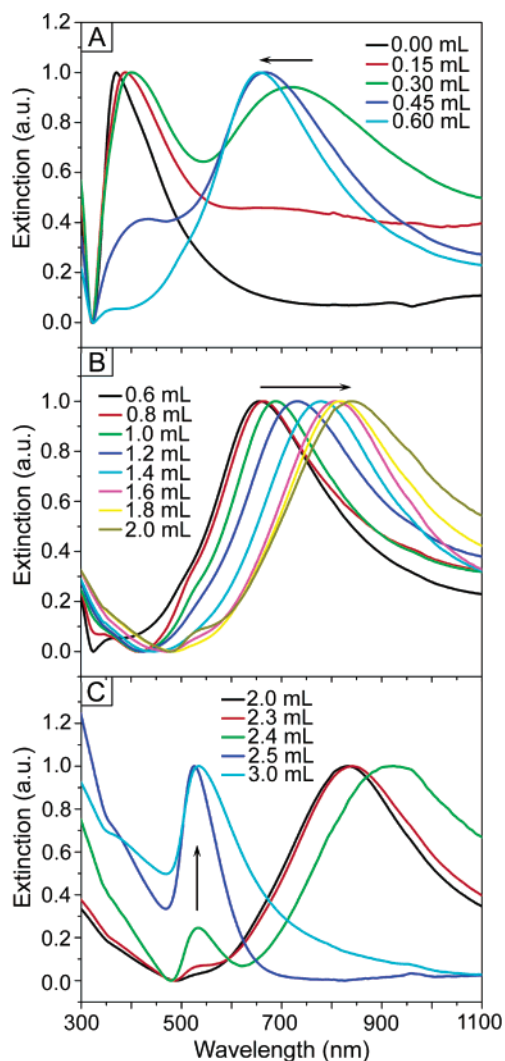
Figure 8. UV−visible−near-IR extinction spectra of silver nanowires (all in the same amount) before and after they had reacted with different volumes (as indicated on each panel) of 1 mM HAuCl$_4$ aqueous solution. Similar to nanocubes, the reaction could also be separated into three stages: (A) formation of seamless nanotubes composed of Au−Ag alloy; (B) dealloying of the Au−Ag nanotubes; and (C) fragmentation of the nanotubes (with porous walls) into smaller pieces. All spectra have been normalized against the intensities of their strongest peaks.

HAuCl$_4$ that was added to the dispersion of silver nanowires. Similar to silver nanocubes, holes with relatively large sizes (>20 nm) also displayed the square symmetry because their side surfaces were enclosed by {100} planes. Complete dealloying of the alloyed nanotubes eventually resulted in the formation of gold nanoparticles (Figure 7F).

Due to the significant difference in shape between silver nanowires and nanocubes, the spectral changes involved in the transformation from silver nanowires to nanotubes (as shown in Figure 8A) were different from those displayed in Figure 4A for the nanocubes. More specifically, the nanowires only exhibited a major peak around 380 nm, which originated from the transverse mode of SPR. When they were partially converted to tubular nanostructures (as shown in Figure 7B), this peak was slightly red-shifted due to the formation of gold (or Au−Ag alloy) sheath on the surface of each nanowire. At the same time, a new peak at ∼725 nm was gradually formed, which could be attributed to the transverse mode of newly formed tubular strips. As the volume of the HAuCl$_4$ solution was further
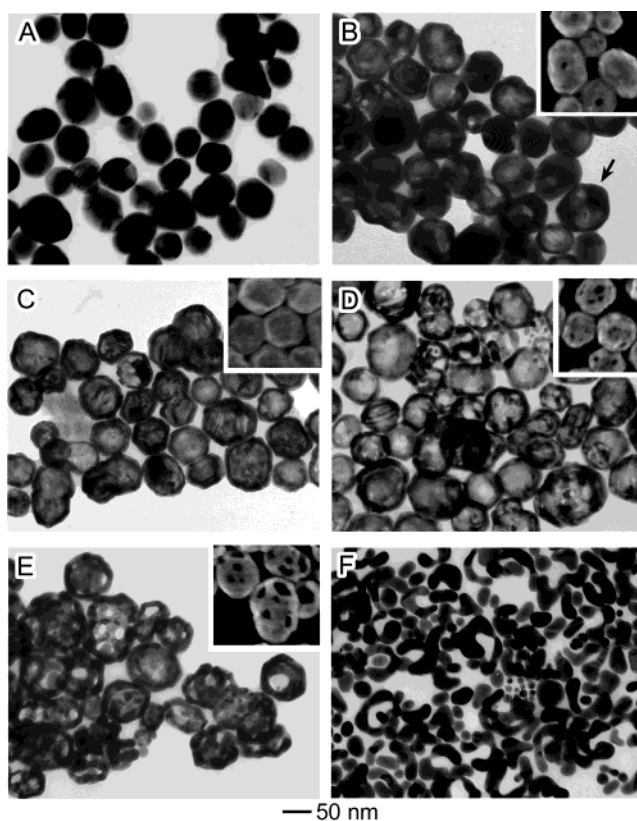
Figure 9. TEM images obtained from spherical silver nanoparticles (A) before and (B−F) after they had reacted with different volumes of 1 mM HAuCl$_4$ solution: (B) 0.25, (C) 0.60, (D) 1.00, (E) 1.20, and (F) 1.50 mL. The arrow in B indicates the formation of holes on the surface and the hollow nanostructure in the interior. The insets of B−E are the corresponding SEM images.

increase to 0.6 mL, the SPR peak of silver nanowires essentially disappeared, indicating that the silver nanowires had been completely transformed into nanotubes. The peak at longer wavelength was blue-shifted back to 655 nm, implying that the nanotubes were increased in wall thickness as the replacement reaction was continued. This result indicated that the resultant gold was homogeneously deposited on the entire surfaces rather than some specific sites. In the dealloying process, the Au−Ag nanotubes exhibited some spectral changes similar to the Au−Ag nanobox system due to the formation of pores in the walls. The SPR peak of nanotubes could be tuned over the range from 655 to 930 nm before they collapsed into gold nanoparticles (as shown in Figure 8B,C).

Galvanic Replacement Reaction between Silver Nanospheres and HAuCl$_4$. Similar morphological and spectral changes were also observed when silver nanospheres were used as templates to react with HAuCl$_4$ solution at 100 °C. The TEM and SEM (all the insets) images in Figure 9 clearly depict the morphologies of products obtained at various stages of the reaction: solid silver nanoparticles (Figure 9A); hollow nanoparticles with holes in their surfaces and small void sizes (Figure 9B); seamless nanoshells with uniform and homogeneous walls (Figure 9C); porous nanoshells with small pinholes (Figure 9D); nanocages with larger pores (Figure 9E); and fragments of gold (Figure 9F). These images were also consistent with the mechanism illustrated in Figure 6. This demonstration suggests that the galvanic replacement reaction could also be well-applied to silver nanostructures with poor crystallinity and poorly

Figure 10. Photographs of aqueous dispersions of silver nanoparticles with spherical shape (see Figure 9A for a TEM image) before and after they had reacted with different volumes of 1 mM HAuCl₄ solution (from left to right): 0, 0.15, 0.25, 0.4, 0.6, 0.8, 1.0, 1.15, and 1.2 mL. Their major extinction peaks were located at 425, 451, 665, 705, 751, 793, 885, 990, and 1030 nm, respectively.

defined shapes, not just to single crystals (nanocubes) or simply twined crystals (nanowires).

These nanostructures with a more or less spherical shape could also be used to tune the SPR peak over a broad range from 425 to 1030 nm. Figure 10 shows the photograph of nine aqueous dispersions of such nanostructures, showing that the color could be tuned to change from yellow to blue to colorless. The tuning in optical properties was mainly accomplished by the structural transformation from solid silver nanoparticles, through seamless Au−Ag alloyed nanoshells, to Au−Ag alloyed nanocages with pores on their surfaces. This demonstration of optical tuning makes it much easier to scale-up the preparation of metal nanostructures with high extinction coefficients in the near-IR region because a rich variety of methods have already been developed to synthesize silver nanoparticles on the scale of commercial usage.[36]

6. Conclusion

We have systematically investigated the morphological, structural, compositional, and spectral changes involved in the galvanic replacement reaction between silver nanostructures and HAuCl₄ in aqueous medium. Two distinctive steps have been resolved: In the first step, the silver nanostructures were continuously dissolved and the resultant elemental gold was epitaxially deposited on the surface of each template. At the same time, the gold layer was transformed into Au−Ag alloy because of the fast interdiffusion between gold and silver at 100 °C. A combination of these two processes led to the formation of well-defined nanostructures which had hollow interiors, smooth surfaces, and homogeneous walls consisting of the Au−Ag alloy. In the second step, the Au−Ag walls were dealloyed as the replacement reaction continued to proceed, and processes such as Ostwald ripening would induce morphological reconstruction, as well as the formation and enlargement of pinholes in the walls. Complete dealloying eventually forced

the porous nanostructures to collapse into gold fragments characterized by irregular shapes. The reaction temperature was found to play a critical role in determining the final morphology of the product. At room temperature, for example, the simultaneous formation of AgCl solid could disrupt the epitaxial deposition of gold atoms on the surfaces of silver templates. The slow diffusion of Ag and Au atoms at such a low temperature also prevents the resultant nanostructures from smoothening their surfaces via processes such as alloying and Ostwald ripening.

The hollow nanostructures with controllable morphologies and structures could be used to tune their SPR peaks from 400 to 1200 nm, a spectral region that covers the wavelengths of both visible and near-IR. The near-IR region is particularly interesting in biomedical applications because photons with wavelengths in this region can harmlessly pass through soft biological tissues. Due to the high extinction coefficients associated with metal nanostructures described in this work, the near-IR photons could also be converted to phonons (or heat) at high yields. As a result, these nanostructures are expected to find use as ideal photothermal converters in a range of applications that include photothermal cancer therapy and photothermally triggered drug release. Even though these nanostructures were made with hollow interiors and pores in their surfaces, the high crystallinity associated with these nanostructures also makes them sufficiently robust for many other applications that include clinical diagnostics, catalysis, optics, electronics, and optoelectronics.

(36) (a) Silvert, P.-Y.; Herrera-Urbina, R.; Duvauchelle, N.; Vijayakrishnan, V.; Elhsissen, K. T. *J. Mater. Chem.* **1996**, *6*, 573. (b) Silvert, P.-Y.; Herrera-Urbina, R.; Tekaia-Elhsissen, K. *J. Mater. Chem.* **1997**, *7*, 293. (c) Schmid, G. *Chem. Rev.* **1992**, *92*, 1709. (d) Goia, D. V.; Matijevic, E. *New J. Chem.* **1998**, *22*, 1203.